ECMWF Feature article

from Newsletter Number 154 – Winter 2017/18

METEOROLOGY

Why warm conveyor belts matter in NWP

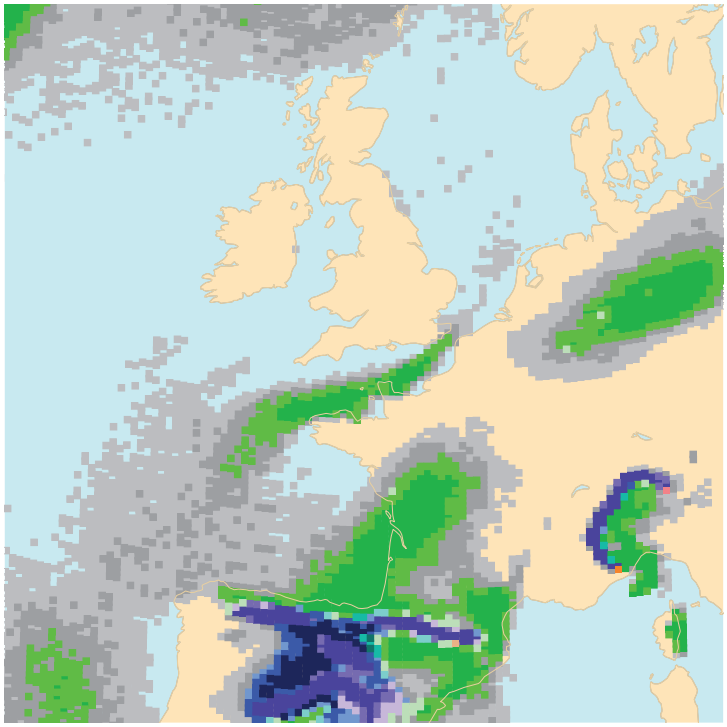

www.ecmwf.int/en/about/news-centre/media-resources

doi:10.21957/mr20vg

This article appeared in the Meteorology section of ECMWF Newsletter No. 154 – Winter 2017/18, pp. 21-28.

Why warm conveyor belts matter in NWP

Mark Rodwell, Richard Forbes, Heini Wernli (ETH Zurich)

A warm conveyor belt (WCB) is a coherent warm and moist airstream, which originates in the boundary layer of an extratropical cyclone's warm sector. Air within the WCB ascends in a day or two to the upper troposphere while moving poleward. WCBs are the primary cloud- and precipitation-generating flow in extratropical cyclones, and they can be associated with extreme precipitation. In this article, based on work carried out jointly with ECMWF Fellow Heini Wernli and his team at ETH Zurich and discussed at a recent bilateral meeting, we illustrate two more ways in which WCBs are important in numerical weather prediction (NWP): The microphysical processes they involve can have a strong impact on the larger-scale dynamics and they are a major source and magnifier of forecast uncertainty.

Correctly modelling WCBs is of great relevance to ECMWF's Strategy to 2025, which calls for improved forecasts of extreme weather and regime transitions and increased reliability and sharpness of ECMWF ensemble forecasts. Here we suggest two ways to improve the representation of WCBs in weather models: better cloud microphysics and improvements in the initialisation of humidity.

An ascending airstream

In the northern hemisphere, WCBs are more frequent in winter than in summer, with two preferential ascending regions in the western North Atlantic and North Pacific. In Figure 1, a WCB is associated primarily with a low-pressure system near Iceland (L). It is seen to transport low values of potential vorticity (PV, blue shading) from the subtropical lower troposphere to the extratropical upper troposphere (Box A). 'WCB trajectories' can be calculated by searching for air parcels that rise more than 600 hPa in 2 days and which, at some time, are coincident with a low pressure system. Green dots show where such ascending air-parcel trajectories intersect with the upper-tropospheric 310 K isentropic surface (the surface of constant potential temperature) and thus contribute to the formation of a large-amplitude upper-level ridge (R). Most of the low-PV air masses forming the ridge ascended cross-isentropically as part of the WCB and experienced intense diabatic heating during the previous one to two days.

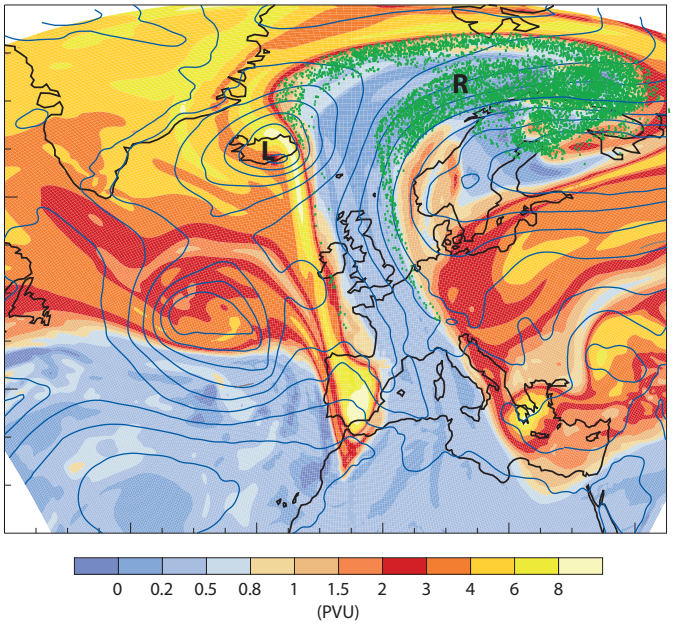

Figure 1 Potential vorticity (PV) on the 310 K isentropic surface (shading), mean sea-level pressure (contour interval 5 hPa) and the locations where 2-day WCB trajectories intersect the 310 K surface (green dots) at 0600 UTC on 31 January 2009. Figure from *Joos & Wernli* (2012).

doi:10.21957/mr20vg

Potential vorticity

A

To a good approximation on synoptic scales, potential vorticity (PV) is the product of the vertical component of the absolute vorticity and the stratification, where absolute vorticity is a measure of the spin of the air and stratification is the vertical gradient in potential temperature (the temperature that air would have if it were brought to a reference pressure of 1,000 hPa). PV is conserved by an air parcel in the absence of friction and diabatic heating.

In the context of WCBs, ascent and poleward mass transport leads to the formation and amplification of upper-level negative PV anomalies, which can cause downstream wave-breaking and the subsequent initiation of periods of calm, 'blocked' conditions.

Figure 2 shows another WCB event over the eastern North Atlantic. Ascending air parcels are shown at various heights along the WCB trajectories (blue, yellow and red circles). The pressure level of cloud tops, indicated by grey shading, and the occurrence of deep convection (green dots) highlight the intense heating taking place. The grey contours show mean sea-level pressure with a low pressure system to the west of the WCB, and the red contour shows 2 PVU potential vorticity at 320 K. Again a ridge can be seen building at the end of the WCB trajectories.

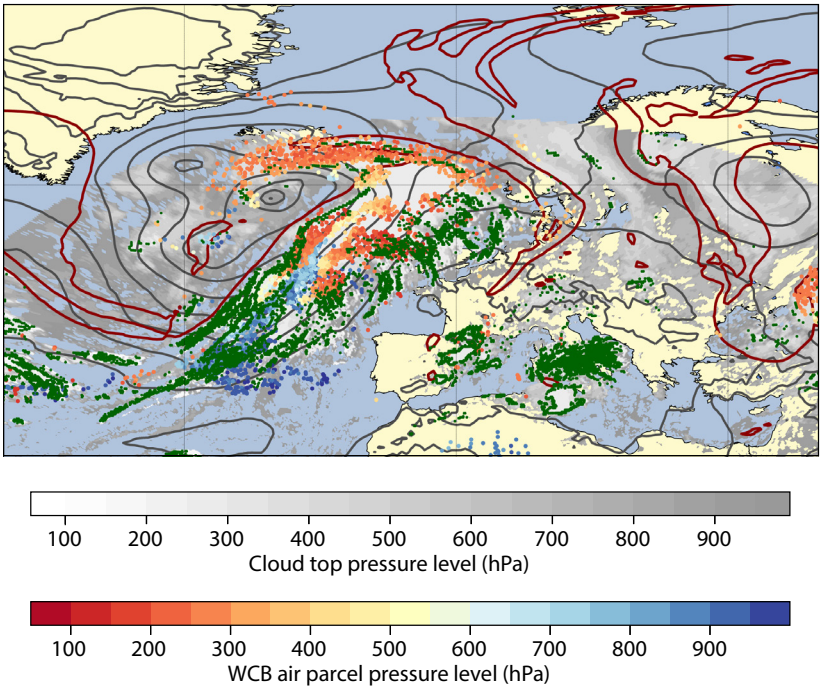

Figure 2 Cloud structure and WCB of cyclone Vladiana at 15 UTC on 23 September 2016. Blue, yellow and red dots indicate the pressure levels of WCB air parcels for this time. The grey shading shows the pressure at cloud-top level and the green dots indicate deep convective clouds based on Meteosat Second Generation satellite data. The grey contours show mean sea-level pressure (with contour interval 5 hPa) and the red contour shows 2 PVU at 320 K. Plot courtesy of Annika Oertel.

Amplification of uncertainties

Poor forecasts for Europe are often associated with the initiation of such ridge events, which can lead to blocking conditions (*Ferranti et al.*, 2015). One such case is shown in Figure 3a for ECMWF high-resolution forecasts (HRES), ensemble forecasts (ENS) and the control forecast (a forecast at ensemble resolution with unperturbed initial conditions and model physics, CTR). Time series of root-mean-square errors (RMSE) for forecasts of European 500 hPa geopotential height at day 6 show a spike in errors for forecasts initiated between about 6 and 7 March 2016. The fact that some ENS members did not suffer large errors suggests that this is a situation of low predictability rather than a situation which the model is unable to represent adequately. Figure 3b shows the differences at day 2 between the five best and the five worst performing members at day 6, a form of 'ensemble sensitivity' experiment. It highlights that the differences at day 6 originate from differences in a trough–ridge feature over the central North Atlantic at day 2. Figure 3c shows the presence of WCB trajectories at this time and location, suggesting that WCBs (including any embedded convection) act to enhance uncertainty in the subsequent forecast flow evolution.

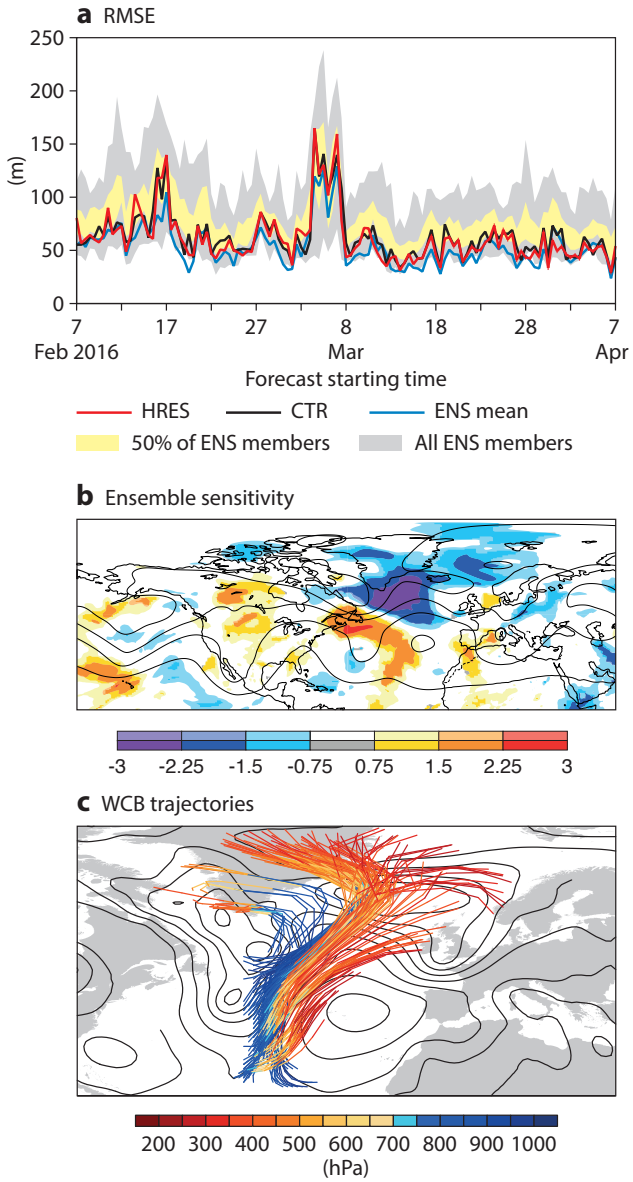

Figure 3 The plots show (a) the evolution of root-mean-square error (RMSE) of 500 hPa geopotential height for ECMWF forecasts over Europe (12.5°W–42.5°E, 35°N–75°N) at day 6, (b) the normalised difference at day 2 of the 5 forecasts with largest RMSE over Europe at day 6 and the 5 members with the smallest RMSE over Europe at day 6, for forecasts starting at 00 UTC on 7 March 2016 (statistically significant differences at the 95% confidence level are shown in bold colours, contours show the ensemble mean of geopotential height at 200 hPa at day 2), and (c) two-day forward WCB air parcel trajectories based on ECMWF analysis data, starting at 00 UTC on 9 March 2016 in the region 70°W–20°W, 20°N–60°N and fulfilling the criterion of ascending more than 550 hPa within 2 days (contours show mean sea-level pressure at 00 UTC on 9 March 2016). Panels (a) and (b) are from *Magnusson* (2017), panel (c) courtesy of Christian Grams, Linus Magnusson and Erica Madonna.

doi:10.21957/mr20vg

Based on very short (12-hour) forecasts within the Ensemble of Data Assimilations (EDA), Figure 4a shows an example of the uncertainty growth rate in PV at 315 K. This is high in the WCB event over the North Atlantic and in the mesoscale convective system (MCS) event over North America, particularly to the north of some of the moist processes depicted by the ensemble-mean precipitation, where the 315 K isentropic surface is closer to the strong PV gradients at the tropopause. In both cases, convective aspects appear to be emphasized. Their combined effect on the forecast was high uncertainty about the formation of a block over Europe by day 6. More systematically, for a composite of many WCB events off the east coast of North America, we can see in Figure 4b that, after one day, such events lead to an increase (approximately a doubling) of uncertainty in upper-tropospheric winds compared to no-WCB events. Results are only plotted for locations where aircraft observations are available; this co-location with observations is important if we are to be able to assess whether this doubling of uncertainty is warranted.

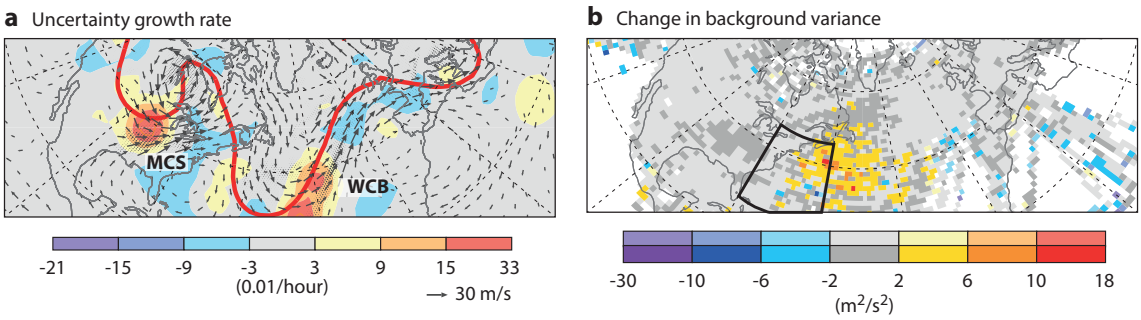

Figure 4 The plots show (a) the one-day mean, centred on 06 UTC on 7 March 2017, of the synoptic-scale uncertainty growth rate (shading) for PV on the 315 K isentropic surface (derived from the background forecasts of the ECMWF Ensemble of Data Assimilations, EDA, and with the transport of uncertainty by the ensemble-mean horizontal winds removed to highlight local sources), the 2 PVU contour on the 315 K surface (red, indicating where this surface intersects the tropopause) and horizontal winds on the 850 hPa surface (vectors) based on the unperturbed control member of the EDA, and the ensemble-mean 24 h accumulated precipitation (dots, with the largest indicating about 50 mm precipitation), and (b) the change in EDA background variance in zonal winds at 200 hPa, co-located with aircraft observations and based on a composite of the 50 strongest WCB events with inflow in the box indicated one day before, and a corresponding composite of 87 non-WCB situations.

Sensitivities to clouds and convection

Latent heating clearly contributes to the ascent within WCB events, but how sensitive are the upper-level PV and downstream impacts to the details of cloud microphysics and convection? Figure 5 shows the upper-level PV structure and the blocking evolution for a WCB event which occurred during the NAWDEX (North Atlantic Waveguide and Downstream Impact Experiment) field campaign in September and October 2016. The left-hand panels show a single control forecast and the right-hand panels show a single forecast where latent heating was artificially turned off in the WCB region within the layer 900–500 hPa. For the control forecast we see that strong ascent leads to upper-level divergent outflow on the western flank of an amplifying ridge. In the event this ridge then broke anticyclonically and led to the onset of blocking conditions. When latent heating is turned off (right-hand panels), the ascent and outflow are reduced, the ridge does not amplify and, in the absence of wave-breaking, the block is not initiated. This example illustrates how the physics within WCBs can play a crucial role in the initiation of blocking anticyclones, and for the upper-level wave dynamics in general.

To consider the consequences of more realistic forecast model deficiencies, Figure 6 shows heating rates due to individual microphysical processes integrated along WCB trajectories for the North Atlantic cyclone investigated by *Joos & Wernli* (2012) and shown in Figure 1. The heating rates were simulated with ECMWF's Integrated Forecasting System (IFS – left) and the regional COSMO (Consortium for Small-scale MOdelling) model (right). There are striking differences between the respective contributions to the total heating from condensation and depositional growth of ice and snow, implying large uncertainties in the details of the cloud microphysics. Note also that convective heating is likely to mean that real air

parcels will deviate from the derived trajectories. Such differences are likely to lead to different trajectory slopes, and thus to differences in the magnitude and latitude of the upper-tropospheric PV anomaly and the subsequent downstream development. For example, *Gray et al.* (2014) highlighted too weak forcing by WCBs as a possible reason for upper tropospheric ridge errors in the IFS.

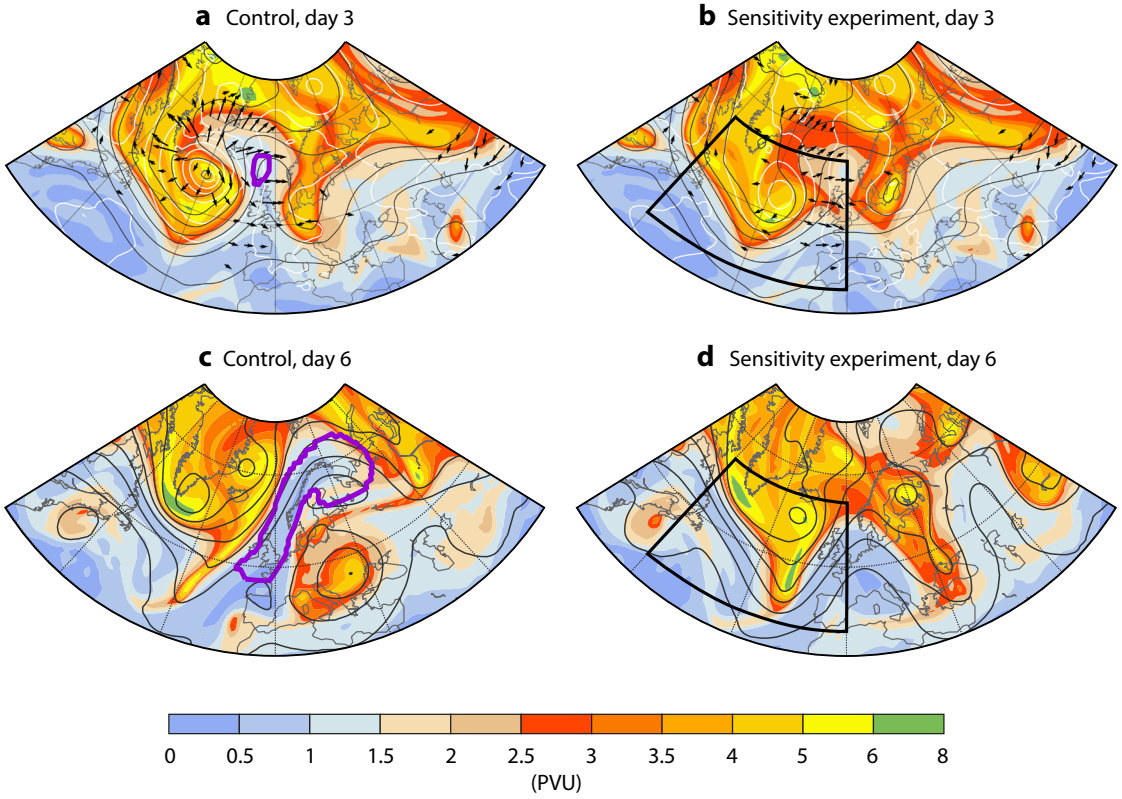

Figure 5 Vertically averaged PV between 500 and 150 hPa (shading), 500 hPa geopotential height (black contours), diagnosed block (purple contour), and vertically-averaged divergent wind between 500–150 hPa (arrows, upper panels only) for (a) the IFS control simulation after 3 days, (b) a sensitivity experiment with latent heating turned off in the box indicated within the layer 900–500 hPa, after 3 days, (c) the control simulation after 6 days, and (d) the sensitivity experiment after 6 days. Plots from work with Daniel Steinfeld, Maxi Boettcher and Stephan Pfahl.

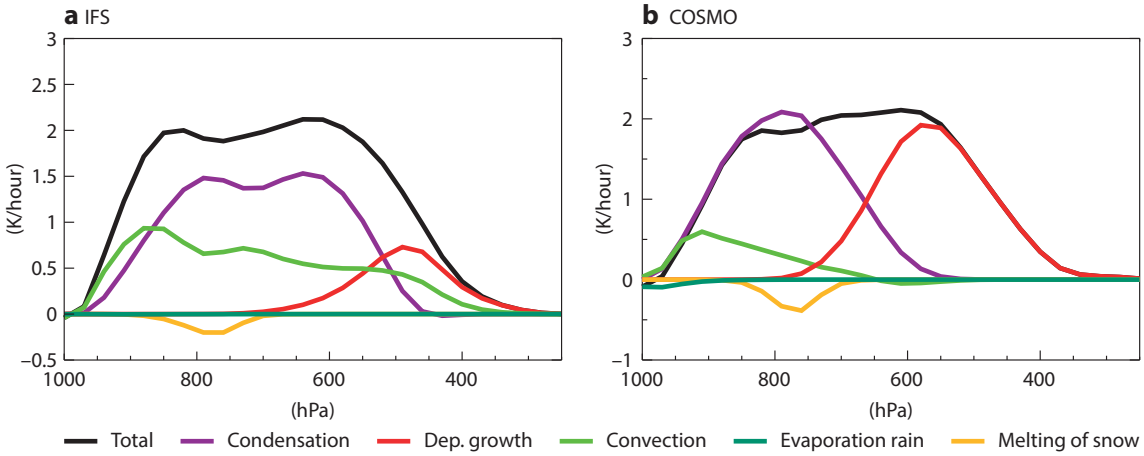

Figure 6 Average diabatic heating rates as a function of pressure, following the WCB trajectories initiated at 06 UTC 29 January 2009 as shown in Figure 1, for each of the dominant physical processes, based on (a) IFS Cycle 41r1 microphysics (adapted from Joos & Forbes, 2016) and (b) the regional COSMO model used in *Joos & Wernli* (2012).

doi:10.21957/mr20vg

The impact on the circulation of uncertainties in cloud microphysics is demonstrated in Figure 7, which shows a snapshot of a rapidly deepening cyclone over the North Pacific, simulated with the IFS. Figure 7a shows lower-tropospheric PV associated with the cyclone on 11 April 2017. As the precipitating air wrapped around and into the cyclone centre, snow sublimation (Figure 7b) and snow melting (Figure 7c) at low levels led to relatively more cooling below than above the 24h back-trajectories of air parcels within this layer, and thus to increased stratification and PV at the level of the parcels. However, further east in the band of descending air beneath the cold frontal region, sublimation (Figure 7b) tends to occur above the parcel trajectories, as the snow falls into the cold dry air from the frontal cloud, and this acts to decrease stratification and PV at the level of the parcels. The melting aspect seems to have less impact on the stratification and PV along the cold front at this level. These results (and more idealised studies such as by *Crezee et al.*, 2017) demonstrate that the details of microphysics can have a significant impact on the material change in PV, and thus potentially on the larger-scale circulation (*Hoskins et al.*, 1985).

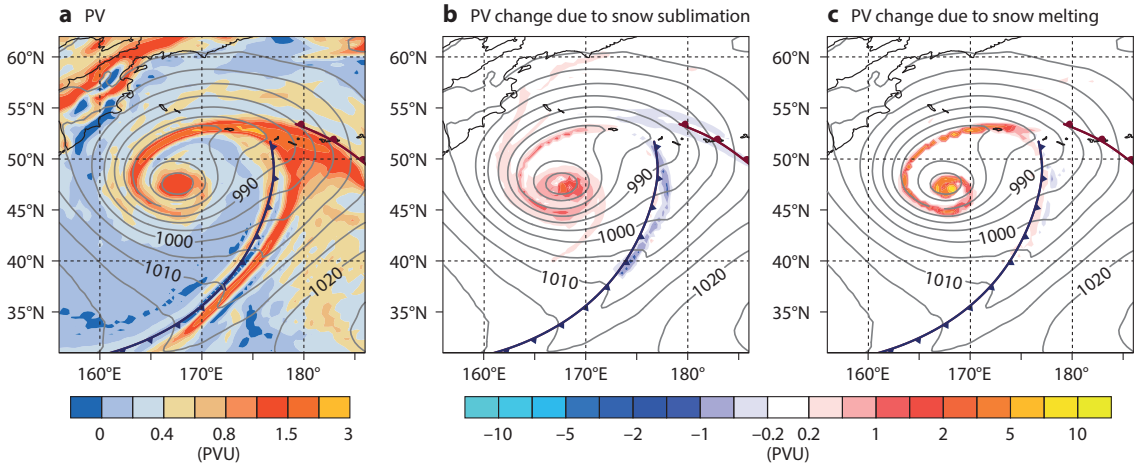

Figure 7 The shading in these plots shows (a) the PV distribution in the lower troposphere (the 950 to 850 hPa layer) for a cyclone in its mature stage (about 2 days after genesis), (b) the change in PV associated with the sublimation of snow over the previous 24 hours, and (c) the change in PV associated with the melting of snow over the previous 24 hours. PV changes are integrated along back-trajectories of air parcels ending up within the lower tropospheric layer. Contours show mean sea-level pressure and the warm and cold fronts are drawn using the usual symbols. The forecast was produced using IFS Cycle 43r1 at a resolution of TCo639. Plots from work with Roman Attinger, Maxi Boettcher and Hanna Joos.

Using observations to identify model deficiencies

Given the importance of WCBs in forecasting and in view of the forecast sensitivities to model formulation, there is a clear potential for forecast model improvement. Observations are key to any such improvement. In numerical weather prediction, millions of observations (conventional in-situ and satellite remote-sensing) are assimilated each day and there is scope to use these to guide the development process. Nevertheless, in cloudy situations such as WCBs, there is a lack of relevant observations and there are difficulties with assimilating existing observations. Hence there is also a need to make use of non-assimilated observations and to undertake dedicated field campaigns.

Radar and lidar data from the ‘A-train’ satellite constellation provide useful information on cloud composition and can be used to diagnose deficiencies in forecast models. In Figure 8 the modelled cloud phase of WCB air parcels is overlaid on CloudSat radar reflectivity observations at 00 UTC on 3 January 2014. Although there is no simple relationship between reflectivity and cloud phase, the high reflectivity values below 6–8 km indicate that the WCB air parcels form part of very strongly precipitating clouds, with snow above and rain or melting snow below the melting layer. In the upper part of the clouds, the lower reflectivity values indicate ice clouds rather than falling snow. This ability to match A-train observations such as CloudSat radar and CALIPSO lidar with WCB events, and the use of observation operators (which map model fields to observations) should help in the diagnosis of modelling deficiencies. Research to assimilate such radar/lidar data is under way and will be useful for forecast initialisation when the coverage of such observations increases through the EarthCARE satellite programme.

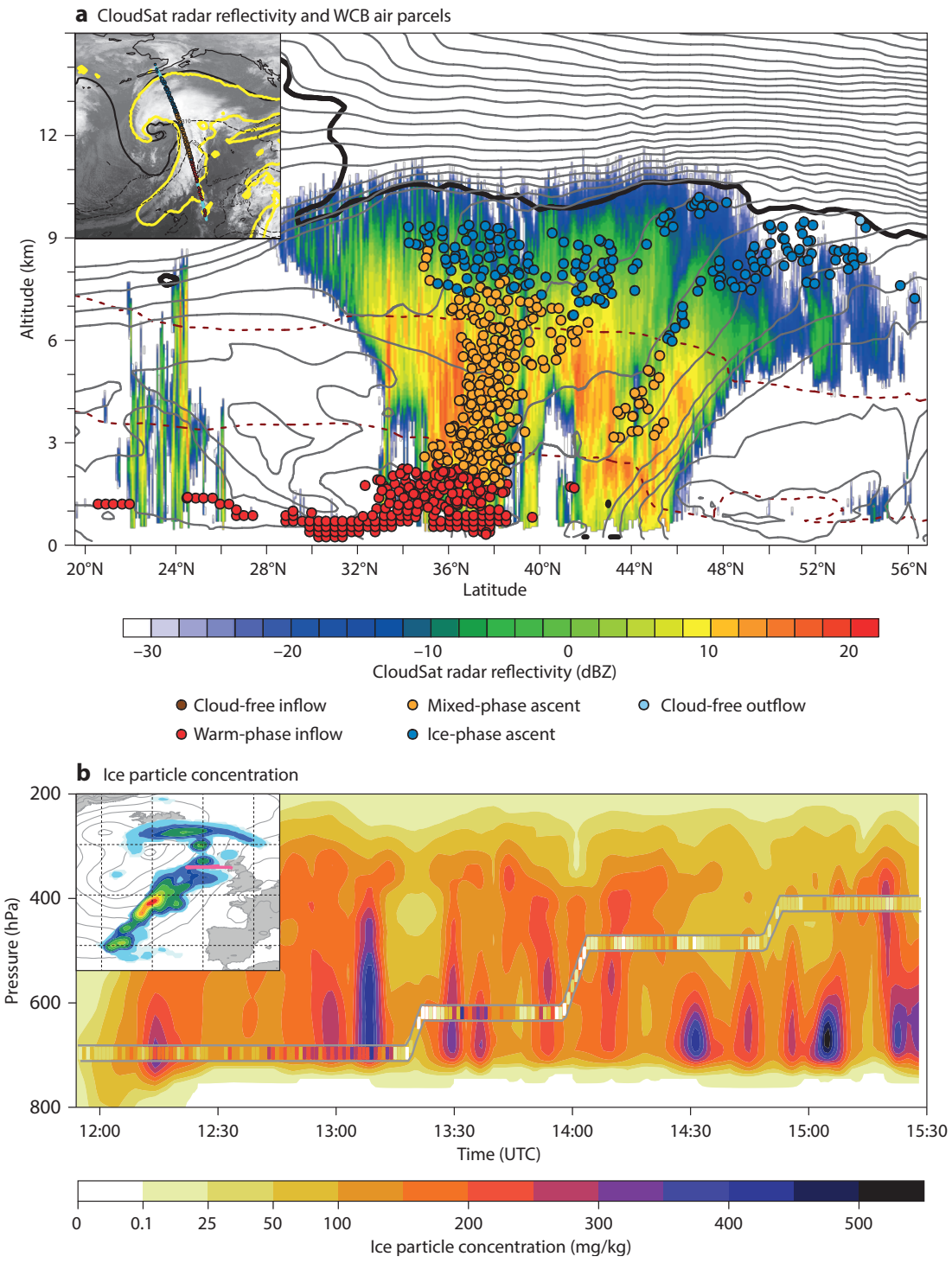

Figure 8 The plots show (a) CloudSat radar reflectivity (shading) at 00 UTC on 3 January 2014, for a cross section of the atmosphere along the line shown in the inset, together with ECMWF operational analyses of interpolated equivalent potential temperature (black contours every 5 K), temperature (red dashed contours at 0° and -23°C), the 2 PVU contour (thick black line), and the positions of the intersected WCB trajectories, i.e., the WCB air parcels located within less than 20 km of the satellite track (dots, coloured according to their cloud phase), and (b) in-situ ice particle concentration as a function of time and height on 23 September 2016 from Nevzorov probe observations on board the BAe146 FAAM aircraft during the NAWDEX field campaign as it flew across a WCB associated with cyclone Vladiana (inset). These are overlaid onto the profile of corresponding ice particle concentrations (the sum of cloud ice and snow) based on the ECMWF operational forecast starting at 12 UTC. The in-situ measurements are averaged over 60 s and the forecast data has 1 h temporal resolution and 0.5° spatial resolution. Panel (a) is from *Binder* (2017) and panel (b) is based on work with Elisa Spreitzer, Maxi Boettcher and Hanna Joos, in collaboration with Geraint Vaughan and Chris Dearden (aircraft data).

doi:10.21957/mr20vg

Figure 8b shows data from a return flight across the WCB of cyclone Vladiana made on 23 September 2016 during the NAWDEX field campaign. Ice particle concentrations measured by an instrument on the BAe146 FAAM aircraft are plotted in a narrow observation band on top of the corresponding predicted profiles from a short forecast. Note that high concentrations are observed around 1310 UTC when the aircraft first passed through the WCB region. Lower values are then observed on the other side of the WCB at around 1320 UTC before the aircraft returned back through the WCB at around 1330 UTC. These rises and falls in observed concentrations agree qualitatively with those predicted by the short forecast, but there is scope for improvements based on this co-location of observational and short forecast data.

Another intensive observational period during the NAWDEX campaign focused on the strong water vapour transports that are important for downstream high-impact precipitation events. Figure 9 shows water vapour profiles observed by lidar on board the HALO aircraft. The strong low-level humidity along the eastern return leg (within a strong south-westerly flow) is indicative of an 'atmospheric river' (*Lavers et al.*, 2011) and led to heavy precipitation over Scandinavia when strong WCB ascent occurred from this moist filament. Dropsonde data from this and other NAWDEX flights were assimilated in real time into the ECMWF operational analysis, and comparisons with the background forecast and model process tendencies should provide insight into model deficiencies.

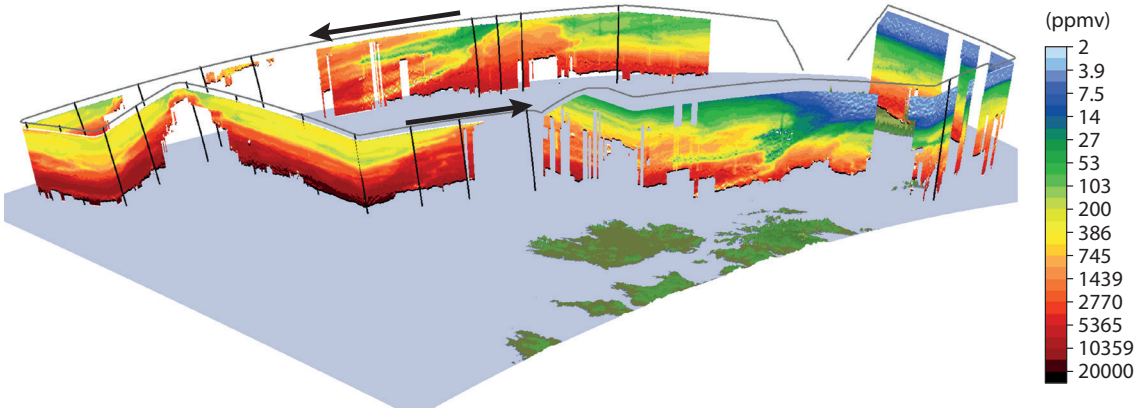

Figure 9 Water vapour profiles as derived from Differential Absorption Lidar (DIAL) observations made from the HALO aircraft on 27 September 2016 as part of the NAWDEX field campaign over the North Atlantic. Figure courtesy of Andreas Schäfler.

Improving the forecast initialisation

It is important to correctly initialise moisture in situations with strong moisture transports in our forecasts (see also *Schäfler & Harnisch*, 2015), but this is difficult to achieve in practice. For example, Figure 10 shows a variance budget applied to the EDA for a composite of the 50 strongest WCB inflow cases off the east coast of North America between November 2015 and October 2016. Here the variance budget is applied to satellite Microwave Humidity Sounder observations of lower-tropospheric humidity and modelled values mapped to these observations. In a 'perfect' forecast system, and with no observation errors, the mean background (short-range forecast) variance (EnsVar, Figure 10c) would match the mean-squared difference between the observations and the ensemble-mean ($Depar^2$, Figure 10a); an example of the so-called 'spread-error' or 'spread-skill' relationship. In reality, while both panels show larger values in the WCB region compared to adjacent regions, the mean ensemble variance (Figure 10c) is smaller than the mean squared departure (Figure 10a). The more accurate relationship, which takes observation uncertainty into account, can be written as

$$Depar^2 = Bias^2 + EnsVar + ObsUnc^2 + Residual, \text{ where } Bias^2$$

and Residual indicate mean and variance deficiencies. What we find for this observational data in WCB situations is that the bias is not significant (Figure 10b) but that our modelled observation uncertainties ($ObsUnc^2$, Figure 10d) are very large, so a large and statistically significant negative residual (Figure 10e) is required to close the budget. The implication is that the observation errors, as modelled within the data assimilation system, are considerably larger than they could be. While the goal would be to reduce these observation error estimates, this may only be sensible after improvements to, e.g., cloud detection

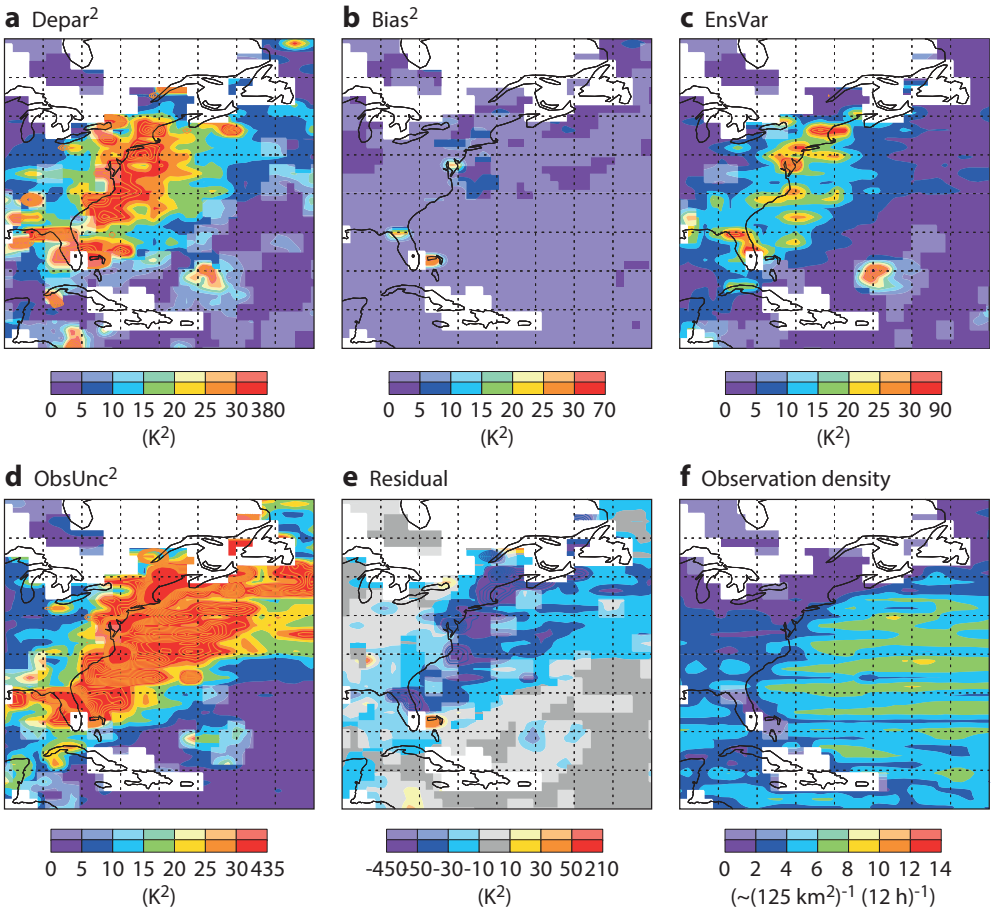

Figure 10 The EDA reliability budget applied to the strongest 50 WCB events off the east coast of North America in the period November 2015 to October 2016, showing (a) the mean-squared difference between the observations and the ensemble-mean ($Depar^2$), (b) the squared estimated bias ($Bias^2$), (c) the mean background variance (EnsVar), (d) the squared observation uncertainty ($ObsUnc^2$, the variance of modelled observation errors), (e) the residual (the variance required to close the budget $Depar^2 = Bias^2 + EnsVar + ObsUnc^2 + Residual$), and (f) the observation density. Saturated colours indicate statistical significance at the 95% confidence level.

doi:10.21957/mr20vg

and modelled boundary-layer heights, due to the deep weighting function of this observation type. This budget can be applied to any observation type and gives useful insight into the initialisation of other model fields including wind, temperature and surface pressure.

Another approach to improved initialisation of humidity might be to focus on upstream surface humidity fluxes (*Pfahl et al.*, 2014) in less cloudy regions. In May 2017, a workshop on the Meteosat Third Generation Infrared Sounder was held at ECMWF. Such hyper-spectral infrared observations from geostationary satellites could provide better humidity profile information with excellent time sampling. Preliminary results show that, provided radiative transfer errors are kept low, the radiance associated with hypothetical elevated humidity in the lower troposphere, e.g. humidity associated with the start of a WCB or an atmospheric river, could potentially be detected.

Future directions

It is clear that WCBs have a major impact on medium-range predictability in the extratropics, in particular as a result of their role in developing downstream ridges, initiating downstream blocking and amplifying uncertainty. It is also clear that improvements could be made to the initialisation and representation of WCBs in current forecasting systems. Promising areas for research and development, already under way, include:

- Improved use of observations by the EDA during WCB events
- Improved representation of physics during WCB events
- Improved ensemble reliability in situations where WCBs exist (or are likely to exist at a future date)
- Continued research into extended-range predictability, including teleconnections between predictable drivers (such as in the tropics), WCB events, and extratropical regime transitions (such as the initiation of blocking)

Work in these areas will benefit from continued collaboration with members of the atmospheric dynamics group at ETH and other scientists with similar interests.

Further reading

Binder, **H.**, 2017: Warm conveyor belts: cloud structure and role for cyclone dynamics and extreme events. PhD thesis, ETH Zurich, No 24016.

Crezee, **B.**, **H. Joos** & **H. Wernli**, 2017: The microphysical building blocks of low-level potential vorticity anomalies in an idealized extratropical cyclone. *J. Atmos. Sci.*, **74**, 1403–1416.

Ferranti, **L.**, **S. Corti** & **M. Janousek**, 2015: Flow-dependent verification of the ECMWF ensemble over the Euro-Atlantic sector. *Quart. J. Roy. Meteorol. Soc.*, **141**: 916–924. doi:10.1002/qj.2411.

Gray, **S.L.**, **C.M. Dunning**, **J. Methven**, **G. Masato** & **J.M. Chagnon**, 2014: Systematic model forecast error in Rossby wave structure. *Geophys. Res. Lett.*, **41**, 2979–2987, doi:1002/2014GL059282.

Hoskins, **B. J.**, **M. E. McIntyre** & **A. W. Robertson**, 1985: On the use and significance of isentropic potential vorticity maps. *Quart. J. Roy. Meteorol. Soc.*, **111**, 877–946.

Joos, **H.** & **H. Wernli**, 2012: Influence of microphysical processes on the potential vorticity development in a warm conveyor belt: A case-study with the limited-area model COSMO. *Quart. J. R. Meteorol. Soc.*, **138**, 407–418, doi: 10.1002/qj.934.

Joos, **H.** & **R. Forbes**, 2016: Impact of different IFS microphysics on a warm conveyor belt and the downstream flow evolution. *Quart. J. R. Meteorol. Soc.*, **142**, 2727–2739.

Lavers, **D.A.**, **R.P. Allan**, **E.F. Wood**, **G. Villarini**, **D.J. Brayshaw** & **A.J. Wade**, 2011: Winter floods in Britain are connected to atmospheric rivers, *Geophys. Res. Lett.*, **38**, L23803, doi:10.1029/2011GL049783.

Madonna, **E.**, **H. Wernli**, **H. Joos** & **O. Martius**, 2014: Warm conveyor belts in the ERA-Interim dataset (1979–2010). Part I: Climatology and potential vorticity evolution. *J. Climate*, **27**, 3–26, doi: 10.1175/JCLI-D-12-00720.1.

Magnusson, **L.**, 2017: Diagnostic methods for understanding the origin of forecast errors. *Quart. J. R. Meteorol. Soc.*, **143**, 2129–2142.

Methven, **J.**, 2015: Potential vorticity in warm conveyor belt outflow. *Quart. J. Roy. Meteor. Soc.*, **141**, 1065–1071, doi:10.1002/qj.2393.

Pfahl, **S.**, **E. Madonna**, **M. Boettcher**, **H. Joos**, & **H. Wernli**, 2014: Warm conveyor belts in the ERA-Interim data set (1979-2010). Part II: Moisture origin and relevance for precipitation. *J. Climate*, **27**, 27–40.

Pfahl, **S.**, **C. Schwierz**, **M. Croci-Maspoli**, **C. M. Grams** & **H. Wernli**, 2015: Importance of latent heat release in ascending air streams for atmospheric blocking. *Nature Geosci.*, **8**, 610–615.

Schäfler, **A.** & **F. Harnisch**, 2015: Impact of the inflow moisture on the evolution of a warm conveyor belt. *Quart. J. R. Meteorol. Soc.*, **141**, 299–310, doi: 10.1002/qj.2360.